Phase knob for switching steady-state behaviors from bistability to multistability via spontaneously generated coherence

Zhonghu Zhu,[1] Ai-Xi Chen,[2] Wen-Xing Yang,[1,3,*] and Ray-Kuang Lee[3]

[1]*Department of Physics, Southeast University, Nanjing 210096, China*
[2]*Department of Applied Physics, School of Basic Science, East China Jiaotong University, Nanchang 330013, China*
[3]*Institute of Photonics Technologies, National Tsing-Hua University, Hsinchu 300, Taiwan*
**Corresponding author: wenxingyang@seu.edu.cn*

Received May 14, 2014; revised July 8, 2014; accepted July 8, 2014;
posted July 9, 2014 (Doc. ID 212078); published August 6, 2014

We conducted a theoretical investigation of the optical steady-state behavior in N four-level Y-type atoms driven coherently by a probe laser and a single elliptically polarized field (EPF) by means of a unidirectional ring cavity. It was found that the optical bistability can be observed for a wide regime of frequency detuning of the probe field, intensity of the EPF, and the atomic cooperation parameter. Interestingly, in principle the optical steady-state behavior can be switched from optical bistability to multistability or vice versa by adjusting the phase difference between two components of the polarized electric field of the EPF if the perfect spontaneously generated coherence of atoms is included. Our results illustrate the potential to utilize EPF for all-optical switching in atomic systems through the phase control, as well as provide guidance in the design for possible experimental implementations.

OCIS codes: (160.4330) Nonlinear optical materials; (190.1450) Bistability.
http://dx.doi.org/10.1364/JOSAB.31.002061

1. INTRODUCTION

The spontaneous emission effect of excited atoms is a general process in light–matter interactions. It is responsible for many important physical phenomena that have been discovered in quantum optics [1]. Over the past few decades, many efforts have been put into finding an approach for the reduction and cancellation of spontaneous emissions of an excited atomic system. However, now it is well known that the closely lying levels of the excited atom can produce new types of coherence via interaction with the vacuum of the radiation field [2–10]. This coherence, called spontaneously generated coherence (SGC), can modify the transient and steady-state response of the medium. In these regards, we note that the effects of SGC on the optical steady-state behaviors in atomic systems have been widely analyzed, and such studies have investigated gain without population inversion [11,12], the evolution of the dark state [13], and the enhanced nonlinearity [14–16]. Especially, it should be noted that the behaviors of optical bistability (OB) and multistability (OM) in atomic systems also can be modified by the SGC effect [17–26], such as the threshold and the shape of the bistable hysteresis cycle.

On the other hand, the relative phase of coherent driving fields has been widely used for controlling several important processes in atomic, molecular, and solid-state systems [27–31], which is usually termed phase control. Recently, intensive interest has been given to the phase control of steady-state behaviors in the presence of the SGC effect. Menon and Agarwal [6] have shown that the SGC brings about quantitative changes in line profiles of absorption and dispersion, and this leads to the dependence of line shapes on the relative phase between the two applied fields when the two applied fields are both strong enough. Wu and Gao [11] have found that the inversionless gain will be related to the relative phase between the probe and the coherent driving fields when an incoherent process is used to pump a Λ atomic system. Furthermore, the phase effect on the optical steady-state behaviors including OB and OM have also been studied in atomic systems confined in an optical ring cavity [19–21]. For example, Gong and co-workers [19,20] showed that the phase fluctuation of the control field leads to OB even when both fields are in resonance with the three-level atoms, and the threshold intensity can be controlled by changing the bandwidth of the control field. Hu and Xu [21] have suggested a method for achieving phase control of the amplitude-fluctuation-induced OB with two-photon resonance in such three-level atoms.

In this paper, we analyze the optical steady-state behaviors via SGC in N four-level Y-type atoms driven coherently by a probe laser and a single elliptically polarized field (EPF) by means of a unidirectional ring cavity. Our results show that the intensity of the EPF driving field and the atomic cooperation parameters can efficiently modify the threshold and the shape of the bistable hysteresis cycle even in the absence of a perfect SGC effect. Moreover, adjustments of the frequency detuning of the probe laser can be used to switch on or off the OB phenomenon. More interestingly, our results also reveal that the conversion between OB and OM can be realized by adjusting the phase difference between the two components of the polarized electric field of the EPF in the presence of a perfect SGC effect. Different from the relative phase between the probe and control fields, the phase difference between the two electric components of the EPF can be changed easily by using the wave plates.

2. MODEL AND MOTION EQUATIONS

Let us consider a four-level Y-type atomic system driven by a linear-polarized probe field and a single EPF, as shown in Fig. 1. The linear-polarized probe field E_p (with angular frequency ω_p) couples the electric dipole transitions between levels $|2\rangle$ and $|3\rangle$ (with transition frequency ω_{23}). A single EPF E_c (with angular frequency ω_c) drives the electric dipole transitions between levels $|1\rangle$ and $|2\rangle$ (with transition frequency ω_{12}) and between levels $|4\rangle$ and $|2\rangle$ (with transition frequency ω_{42}). The utilization of a quarter-wave plate (QWP) can obtain the σ-polarization of the EPF [32]. An initial σ-polarized field E_c with a rotating angle ϕ can be elliptically polarized after entering into the QWP. Thus, the EPF can be decomposed as $E_c = E_c^+\sigma^+ + E_c^-\sigma^-$ with the unit basis vectors σ^- and σ^+, where $E_c^+ = (E_c/\sqrt{2})(\cos\phi + \sin\phi)e^{i\phi}$ and $E_c^- = (E_c/\sqrt{2})(\cos\phi - \sin\phi)e^{-i\phi}$. The amplitudes and the phase difference between two components of the polarized electric field, which is denoted by the rotating angle ϕ for convenience, can be modulated by the QWP.

Inspecting the system, we find that states $|3\rangle$, $|2\rangle$, and $|4\rangle$ are in a typical three-state cascade-type scheme while $|3\rangle$, $|2\rangle$, and $|1\rangle$ compose another cascade-type scheme. Hence, the Y-type system is composed of two cascade-type configurations, and both of them share the ground state $|3\rangle$ and lower excited state $|2\rangle$. The medium is subject to an applied longitudinal magnetic field B that removes the degeneracy of the states $|1\rangle$ and $|4\rangle$, whose Zeeman shift is determined by $\Delta_c = \mu_B m_F g_F B/\hbar$, where μ_B is the Bohr magneton, g_F is the gyromagnetic factor, and $m_F = \pm 1$ is the magnetic quantum number of the corresponding state.

By choosing $H_0 = \omega_p|2\rangle\langle 2| + (\omega_c + \omega_p)|1\rangle\langle 1| + (\omega_c + \omega_p)|4\rangle\langle 4|$ and taking level $|3\rangle$ as the energy origin, under the dipole and rotating-wave approximation, the interaction Hamiltonian of the present atomic system is given by ($\hbar = 1$):

$$H_{\rm int} = (\Delta_c + \Delta_p)|1\rangle\langle 1| + (\Delta_p - \Delta_c)|4\rangle\langle 4| + \Delta_p|2\rangle\langle 2| - [\Omega_p|2\rangle\langle 3| + \Omega_c^+|1\rangle\langle 2| + \Omega_c^-|4\rangle\langle 2| + \text{H.c.}], \quad (1)$$

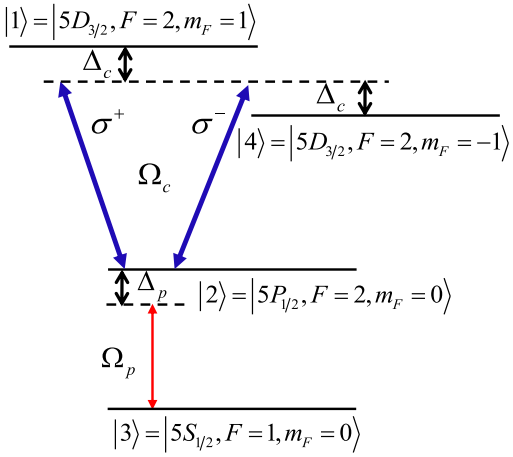

Fig. 1. Four-level Y-type atomic system interacting with a linear-polarized probe field Ω_p (with angular frequency ω_p) and a single elliptically polarized control field Ω_c (with angular frequency ω_c). The frequency detunings of the system are correspondingly defined by Δ_c and Δ_p. A realistic candidate for the proposed atomic system can be found in ^{87}Rb atoms with the designated states chosen as follows: $|5S_{1/2}, F = 1, m_F = 0\rangle$ as $|3\rangle$, $|5P_{1/2}, F = 2, m_F = 0\rangle$ as $|2\rangle$, $|5D_{3/2}, F = 2, m_F = -1\rangle$ as $|4\rangle$, and $|5D_{3/2}, F = 2, m_F = 1\rangle$ as $|1\rangle$.

where $\Delta_p = \omega_{23} - \omega_p$ is the frequency detunings of the probe field. The symbol H.c. represents the Hermitian conjugation. $\Omega_c^+ = -\mu_{12}E_c^+/\hbar = \Omega_c(\cos\phi + \sin\phi)e^{i\phi}$ and $\Omega_c^- = -\mu_{42}E_c^-/\hbar = \Omega_c(\cos\phi - \sin\phi)e^{-i\phi}$ are the half Rabi frequencies of the two components of the EPF, where $\Omega_c = -\mu E_c/\sqrt{2}\hbar$. $\Omega_p = \mu E_p/2\hbar$ is the half Rabi frequency of the probe field with $\mu_{ij} = \mu$ denoting the dipole matrix moment for the relevant optical transition from level $|i\rangle$ to level $|j\rangle$. Then, the density matrix equations of the system can be obtained under the standard approach [1]:

$$\dot\rho_{11} = -\gamma_1\rho_{11} + i\Omega_c^+\rho_{21} - i(\Omega_c^+)^*\rho_{12} - \frac{\eta}{2}\sqrt{\gamma_1\gamma_2}(\rho_{14} + \rho_{41}), \quad (2)$$

$$\dot\rho_{22} = -\gamma_3\rho_{22} + \gamma_1\rho_{11} + \gamma_2\rho_{44} + i(\Omega_c^+)^*\rho_{12} - i\Omega_c^+\rho_{21} + i\Omega_p\rho_{32} - i\Omega_p^*\rho_{23} + i(\Omega_c^+)^*\rho_{42} - i\Omega_c^+\rho_{24} + \eta\sqrt{\gamma_1\gamma_2}(\rho_{41} + \rho_{14}), \quad (3)$$

$$\dot\rho_{44} = -\gamma_2\rho_{44} + i\Omega_c^-\rho_{24} - i(\Omega_c^-)^*\rho_{42} - \frac{\eta}{2}\sqrt{\gamma_1\gamma_2}(\rho_{14} + \rho_{41}), \quad (4)$$

$$\dot\rho_{12} = -\left(\frac{\gamma_1}{2} + \frac{\gamma_3}{2} + i\Delta_c\right)\rho_{12} - i\Omega_c^+(\rho_{11} - \rho_{22}) - i\Omega_p^*\rho_{13} - i\Omega_c^-\rho_{14} - \frac{\eta}{2}\sqrt{\gamma_1\gamma_2}\rho_{42}, \quad (5)$$

$$\dot\rho_{13} = -\left[\frac{\gamma_1}{2} + i(\Delta_c + \Delta_p)\right]\rho_{13} + i\Omega_c^+\rho_{23} - i\Omega_p\rho_{12} - \frac{\eta}{2}\sqrt{\gamma_1\gamma_2}\rho_{43}, \quad (6)$$

$$\dot\rho_{14} = -\left(\frac{\gamma_1}{2} + \frac{\gamma_2}{2} + 2i\Delta_c\right)\rho_{14} + i\Omega_c^+\rho_{24} - i(\Omega_c^-)^*\rho_{12} - \frac{\eta}{2}\sqrt{\gamma_1\gamma_2}(\rho_{11} + \rho_{44}), \quad (7)$$

$$\dot\rho_{23} = -\left(\frac{\gamma_3}{2} + i\Delta_p\right)\rho_{23} + i(\Omega_c^+)^*\rho_{13} + i\Omega_p(\rho_{33} - \rho_{22}) + i(\Omega_c^-)^*\rho_{43}, \quad (8)$$

$$\dot\rho_{42} = -\left(\frac{\gamma_2}{2} + \frac{\gamma_3}{2} - i\Delta_c\right)\rho_{42} - i\Omega_c^+\rho_{41} - i\Omega_p^*\rho_{43} + i\Omega_c^-(\rho_{22} - \rho_{44}) - \frac{\eta}{2}\sqrt{\gamma_1\gamma_2}\rho_{12}, \quad (9)$$

$$\dot\rho_{43} = -\left[\frac{\gamma_2}{2} + i(\Delta_p - \Delta_c)\right]\rho_{43} + i\Omega_c^-\rho_{23} - i\Omega_p\rho_{42} - \frac{\eta}{2}\sqrt{\gamma_1\gamma_2}\rho_{13}, \quad (10)$$

together with $\rho_{ji} = \rho_{ij}^*$ and $\sum_{j=1}^4\rho_{jj} = 1$, where the total decay rates of the above density matrix equations that are added phenomenologically are denoted by $\gamma_i (i = 1\text{–}3)$. It is worthwhile to point out that the SGC effect is taken into account in the present system, since the dipole moments μ_{42} and μ_{12} are not orthogonal and can be obtained from the mixing of the levels arising from internal fields or external microwave fields [2–10] and the energy space between the two lower

levels is very small, which is necessary for the existence of the SGC effect. The term $(\eta/2)\sqrt{\gamma_1\gamma_2}(\eta = \mu_{42}\mu_{12}/|\mu_{42}||\mu_{12}|)$ in the above equations denotes the SGC effect between the spontaneous transitions $|4\rangle\leftrightarrow|2\rangle$ and $|1\rangle\leftrightarrow|2\rangle$. If the two induced dipole moments μ_{42} and μ_{12} are orthogonal, there is no interference and $\eta = 0$. But, if the two dipole moments μ_{42} and μ_{12} are parallel, the interference is maximum and $\eta = 1$.

Now, we consider a medium of length L composed by the atomic sample described above, which is embedded in a unidirectional ring cavity (see [33] p. 71 and references therein), as shown in Fig. 2. For simplicity, we assume that both mirrors 3 and 4 have a 100% reflectivity, and the intensity reflection and transmission coefficients for mirrors 1 and 2 are R and T (with $R + T = 1$), respectively. The propagation of the pulsed probe field in such a medium is governed by Maxwell's wave equation:

$$\nabla^2\vec{E} - \frac{1}{c^2}\frac{\partial^2\vec{E}}{\partial t^2} = \frac{1}{\varepsilon_0 c^2}\frac{\partial^2\vec{P}}{\partial t^2}, \tag{11}$$

with

$$\vec{P} = N[\vec{\mu}_{23}\rho_{32}e^{i(\vec{k}_p\vec{r}-\omega_p t)} + (\vec{\mu}_{12}\rho_{21} + \vec{\mu}_{42}\rho_{24})e^{i(\vec{k}_c\vec{r}-\omega_c t)} + \text{c.c.}], \tag{12}$$

where only the probe field E_p circulates inside an optical cavity, and then under the slowly varying envelope approximation, Maxwell's equation can be reduced to the first-order equation. Thus, we can obtain the relevant propagating equation characterizing the probe field [1]:

$$\frac{1}{c}\frac{\partial E_p}{\partial t} + \frac{\partial E_p}{\partial z} = i\frac{\omega_p}{2c\varepsilon_0}P(\omega_p), \tag{13}$$

where the parameters c and ε_0 represent the velocity of light in a vacuum and the vacuum dielectric constant, respectively. $P(\omega_p) = N\mu_{23}\rho_{32}$ is the slowly oscillating term for the induced polarization in the transition $|2\rangle\leftrightarrow|3\rangle$, with N the atom number density in the atomic sample. In the steady-state case, the time derivative in Eq. (13) $\partial E_p/\partial t$ can be neglected, thus the amplitude of the probe field E_p can be described by

$$\frac{\partial E_p}{\partial z} = i\frac{\omega_p}{2c\varepsilon_0}P(\omega_p). \tag{14}$$

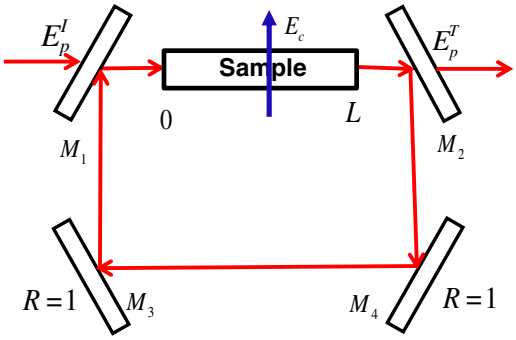

Fig. 2. Schematic setup of the unidirectional ring cavity containing an atomic sample with the length L. E_p^I and E_p^T are the incident and transmitted fields, respectively. E_c represents the EPF control field that is not circulating inside the cavity.

Note that if a set of reasonable parameters for the ring cavity can be found, the input field E_p^I and the transmitted field E_p^T will meet the conditions [33]

$$E_p^T = \sqrt{T}E_p(L), \tag{15}$$

$$E_p(0) = \sqrt{T}E_p^I(L) + RE_p(L), \tag{16}$$

where the term $RE_p(L)$ in Eq. (16) represents a feedback mechanism that results from the reflection of the mirror M_2 and is the main reason for the production of OB or OM. By normalizing the fields ($x = \mu_{23}E_p^T/\hbar\sqrt{T}$ and $y = \mu_{23}E_p^I/\hbar\sqrt{T}$) and using the mean-field approximation [33], the input–output relationship equation can be described by

$$y = x - iC\rho_{23}, \tag{17}$$

where $C = LN\omega_p\mu_{23}^2/2\hbar c\varepsilon_0 T$ is the cooperation parameter for atoms. We should note that the term $iC\rho_{23}$ in Eq. (17) is very important for the OB or OM to occur. From Eq. (17), we find that the expression ρ_{23} is a complicated fractional form of two polynomials. Thus, it is difficult to get a straightforward relationship between the cavity input and output intensities. Therefore, we will solve the density matrix Eqs. (2)–(10) together with the input–output Eq. (17) in the following section.

3. NUMERICAL RESULTS AND PHYSICAL ANALYSIS

In this section, we present typical numerical results for the steady-state solution of the output field in terms of field intensities for different corresponding parameters. As mentioned in the above section, a realistic candidate for the proposed atomic system can be found in ^{87}Rb atoms with the designated states chosen as follows: $|5S_{1/2}, F = 1, m_F = 0\rangle$ as $|3\rangle$, $|5P_{1/2}, F = 2, m_F = 0\rangle$ as $|2\rangle$, $|5D_{3/2}, F = 2, m_F = -1\rangle$ as $|4\rangle$, and $|5D_{3/2}, F = 2, m_F = 1\rangle$ as $|1\rangle$ [34]. To give a clear illustration, we selected $\Delta_c = 7$ MHz $= 0.9\gamma$, $\gamma_1 = \gamma_2 = \gamma$, and $\gamma_3 = 0.01\gamma$, and all the parameters used in the following numerical calculations are in the unit of γ. For simplicity, we assume $\Omega_c^+ = \Omega_c^- = \Omega_c$. Subsequently, as shown in Figs. 3–7, we obtained a few numerical results for the steady behavior of the input–output field intensity with different values of the relevant parameters to illustrate that controllable OB and OM can be achieved in the present four-level Y-type atomic system by means of a unidirectional ring cavity.

In the absence of the SGC effect $\eta = 0$, we analyzed how the frequency detuning of probe field Δ_p and the intensities of the EPF modify the steady-state behavior. In Fig. 3(a), we show the curve diagrams of the input–output field intensity with different frequency detuning Δ_p of the probe field in absence of the SGC effect (i.e., $\eta = 0$), in which the OB behavior can be obviously observed and can be manipulated by the frequency detuning. From Fig. 3(a), it is shown that the bistable threshold and the area of the bistable curve are controllable via changing the frequency detuning Δ_p. It was found that the OB disappears when the probe field is in resonance with the corresponding transition ($\Delta_p = 0$). In contrast, we can see that with increasing Δ_p from γ to 2γ, the bistable threshold increases progressively and the area of the bistable curve becomes wider when all other parameters are kept

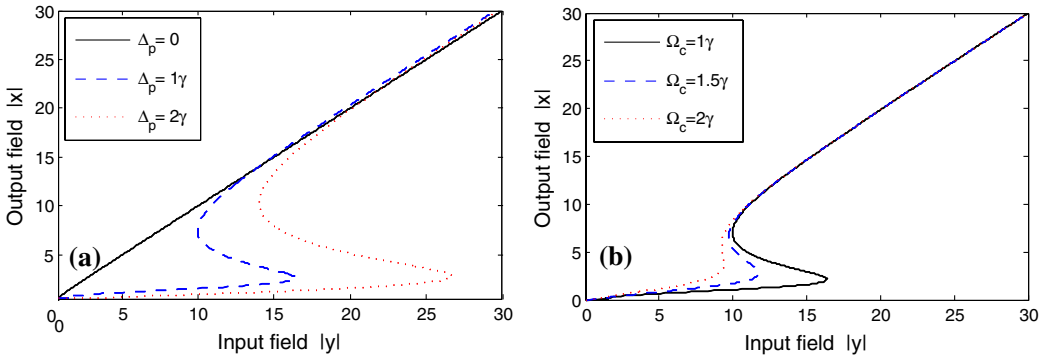

Fig. 3. (a) Curve diagrams of the input–output field intensity with different frequency detuning Δ_p with $\Omega_c = \gamma$. (b) Curve diagrams of the input–output field intensity with different intensities of the elliptically polarized field Ω_c with $\Delta_p = \gamma$. Other values of the parameters were chosen as $\gamma_1 = \gamma_2 = \gamma$, $\gamma_3 = 0.01\gamma$, $\Delta_c = 0.9\gamma$, $C = 100\gamma$, and $\eta = 0$, $\phi = 0$.

fixed. The physics mechanism is rather clear and can be qualitatively explained as follows. By applying the EPF to driving the transitions $|1\rangle\leftrightarrow|2\rangle$ and $|4\rangle\leftrightarrow|2\rangle$, the absorption of the probe field applied to the transition $|2\rangle\leftrightarrow|3\rangle$ and the Kerr nonlinearity of the atomic system can be modified, which leads to a change in the behavior of OB. Thus, it is illustrated here that the absorption-dispersion of the probe field can be modified in the present four-level Y-type atomic system. In Fig. 3(b), we display the effects of the intensity of the EPF Ω_c on the OB behavior without considering the SGC effect (i.e., $\eta = 0$). The data show that the bistable threshold and the area of the bistable curve decrease markedly as the amplitude of the EPF Ω_c increases, which can also be attributed to changes of the absorption-dispersion property resulting from the increases of Ω_c. By applying an increasing intensity of the control field, the absorption of the probe field on the transition $|2\rangle\leftrightarrow|3\rangle$ can be reduced to an extreme extent. Thus, it is even easier for the absorption saturation of the ring cavity to take place.

The observation of the above steady-state behaviors can be interpreted with perturbation theory as follows [1]. First, we can obtain the expression of the first-order solution for ρ_{23} in the steady-state case and the weak probe limit [1,35–40] (i.e., $\Omega_p \ll \Omega_c$ with the assumption of $\rho_{33}^{(0)} \simeq 1$, $\rho_{11}^{(0)} = \rho_{22}^{(0)} = \rho_{44}^{(0)} = 0$). The first-order solution of ρ_{23} is given by

$$\rho_{23}^{(1)} = \frac{i(4bc - \eta^2\gamma_1^2)\Omega_p}{-a\eta^2\gamma_1^2 - 4\eta(\cos(2\phi))^2\gamma_1\Omega_c^2 + 4[abc + (b+c)\Omega_c^2 + (b-c)\sin(2\phi)\Omega_c^2]}, \tag{18}$$

where $a = (\gamma_3/2) + i\Delta_p$, $b = (\gamma_2/2) + i(\Delta_p - \Delta_c)$, and $c = (\gamma_1/2) + i(\Delta_p + \Delta_c)$. From Eq. (18), one can also find the tedious and intricate expressions for the solutions, but without clear insight into the physics. In order to clearly show how the intensity of the EPF Ω_c and the frequency detuning Δ_p affect the OB behavior with neglecting the SGC effect (i.e., $\eta = 0$), according to Eq. (18), the density plot of the probe absorption $\mathrm{Im}(\rho_{23})$ versus Ω_c and the frequency detuning Δ_p is shown in Fig. 4. Specifically, this figure displays the absorption of the probe field on the transition $|2\rangle\leftrightarrow|3\rangle$. As illustrated in Fig. 4, for the case of $\Delta_p = 0$, the absorption of the probe field can be completely suppressed and the atomic system becomes transparent to the weak tunable probe field by increasing the intensity of the control field Ω_c, which can explain why the OB disappeared under $\Delta_p = 0$ at resonance. In addition, with a certain frequency detuning of the probe field, Fig. 4 also demonstrates that the absorption of the probe field on the transition $|3\rangle\leftrightarrow|2\rangle$ and the Kerr nonlinearity can be modified when one increases the control field between the transitions $|2\rangle\leftrightarrow|1\rangle$ or $|2\rangle\leftrightarrow|4\rangle$. As we can see in Fig. 3(b), a smaller threshold intensity comes from the reduction in the effective saturation intensity due to the increasing intensity of the EPF.

It is worth noting that the cooperation parameter C in Eq. (17) is linearly proportional to the atom number density N. One can easily find from Eq. (17) that the cooperation parameter will affect the input–output curves. Thus, we should consider the effect of the cooperation parameter C on the OB behavior. Here, we present how the cooperation parameter C affects the OB behavior for the case of $\eta = 0$. Figure 5 illustrates that the bistable threshold is reduced dramatically as C decreases. From the term $C = LN\omega_p\mu_{23}^2/2\hbar c\varepsilon_0 T$, it can be seen that C changes with N proportionally. Therefore, the decrease of the bistable threshold intensity originates from the probe absorption of the sample, which is enhanced with increasing N. Furthermore, we can optimize the optical switching process for controlling the OB behavior by choosing the electron sheet density of the corresponding system properly [41–46]. We noticed that some works [47–49] reported the influence of the enhanced dipole coupling parameter $g\sqrt{N}$ (with g being the atom-cavity coupling strength) on the OB behavior of multiwave mixing signals in coupled systems consisting of a specific ring cavity and a four-level atom assemble. Those results showed that the OB threshold decreases and the bistable region of the multiwave mixing signal becomes narrow as $g\sqrt{N}$ increases [47], which is different from the influence of the cooperation parameter C on the OB behavior.

As shown in Figs. 3–5, we have demonstrated the creation of the OB and studied the influences of parameters on the

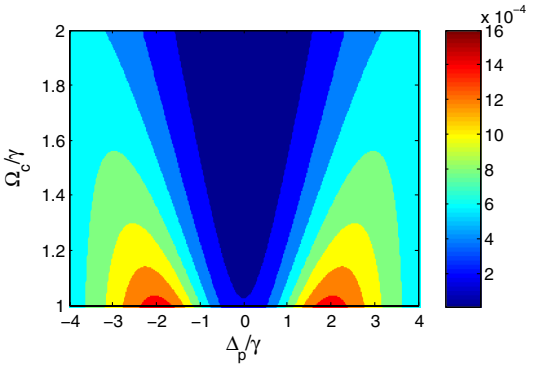

Fig. 4. Density plot of the probe absorption $\mathrm{Im}\,\rho_{23}$ versus the Ω_c and the detuning Δ_p with $\Omega_p = \Omega_p^* = 0.01\gamma$. Other values of the parameters were chosen as $\gamma_1 = \gamma_2 = \gamma$, $\gamma_3 = 0.01\gamma$, $\Delta_c = 0.9\gamma$, and $\phi = 0$, $\eta = 0$.

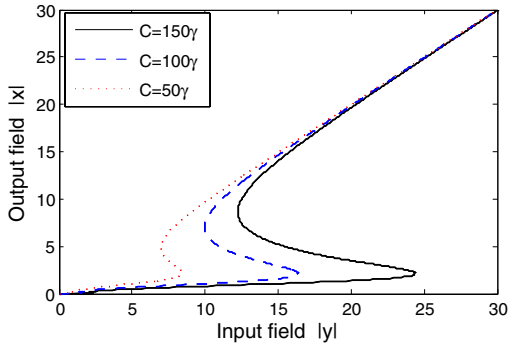

Fig. 5. Curve diagrams of the input–output field intensity with different cooperation parameters C. Other values of the parameters were chosen as $\gamma_1 = \gamma_2 = \gamma$, $\gamma_3 = 0.01\gamma$, $\Delta_c = 0.9\gamma$, $\eta = 0$, $\phi = 0$, and $\Omega_c = \gamma$, $\Delta_p = \gamma$.

bistable behavior in the present atomic system under consideration without including the SGC effect (i.e., $\eta = 0$) and the effect of the phase difference between the two components of the polarized electric field (i.e., $\phi = 0$). However, we should examine the influence of the phase difference ϕ between the two components of the polarized electric field on the optical steady behavior, which is one of the most interesting characteristics of the present atomic system driven by the EPF. In Fig. 6, we present numerical results for the analyses of the SGC effect η and the phase difference between two components of the polarized electric field ϕ on the steady-state of the output field amplitude $|x|$ as a function of input field amplitude $|y|$ for different cases. In contrast to the results of Fig. 3(a), Fig. 6(a) shows that OB output can still be achieved in the presence of the perfect SGC effect (i.e., $\eta = 0.9$) even if the probe resonance condition is satisfied $\Delta_p = 0$. However, the OB phenomenon disappears again when the phase difference ϕ is tuned from $\phi = 0$ to $\phi = 2\pi/3$. For the general case, Fig. 6(b) shows that the bistable threshold increases with an increasing SGC effect η when the phase difference ϕ is equal to zero and the frequency detuning is changed from $\Delta_p = 0$ to $\Delta_p = \gamma$, which demonstrates that the SGC effect can effectively modify the threshold intensity and the hysteresis loop of OB. For fully understanding the influence of the phase difference ϕ on the OB behavior, we plotted Figs. 6(c) and 6(d). As shown in Fig. 6(c), in absence of the SGC effect (i.e., $\eta = 0$), one can find that the OB disappears when the frequency detuning Δ_p and the phase difference ϕ are both equal to zero, which is consistent with the results of Fig. 3(a) (solid line). In contrast, the bistable threshold increases progressively with increasing ϕ from $\pi/3$ to $2\pi/3$ when all other

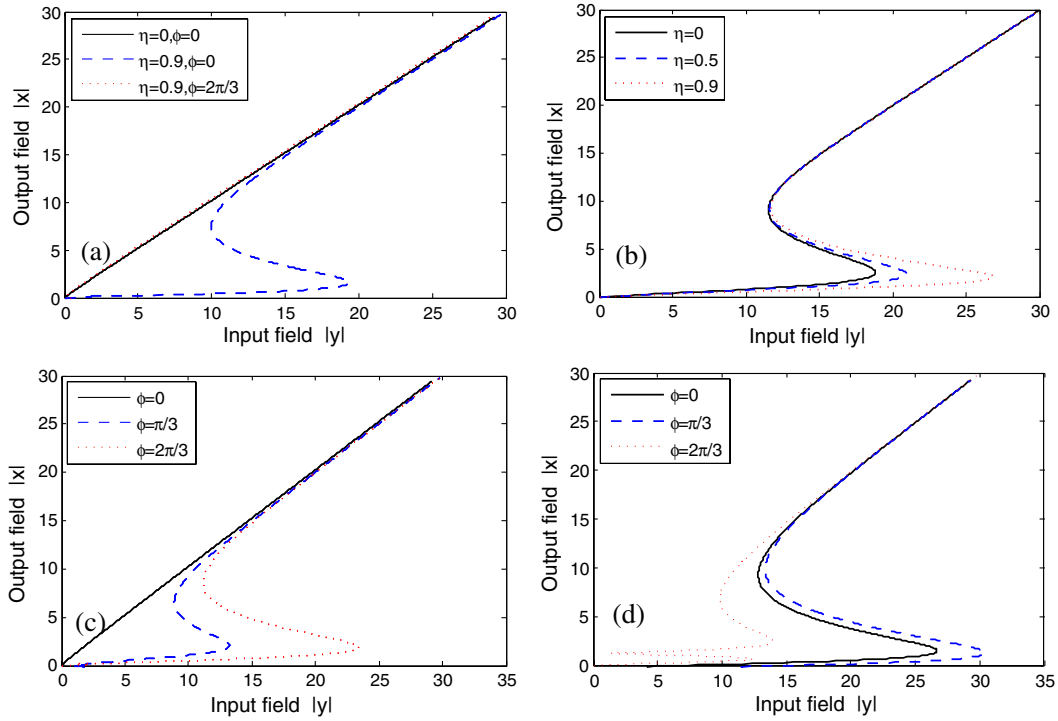

Fig. 6. (a) Curve diagrams of the input–output field intensity for different values of the SGC effect η and different phase differences ϕ between two components of the polarized electric field of the EPF with $\Delta_p = 0$. (b) Curve diagrams of the input–output field intensity for different values of the SGC effect η with $\Delta_p = \gamma$ and $\phi = 0$. (c) Curve diagrams of the input–output field intensity for different phase differences ϕ with $\Delta_p = 0$ and $\eta = 0$. (d) Curve diagrams of the input–output field intensity for different phase differences ϕ with $\Delta_p = \gamma$ and $\eta = 0.9$. Other values of the parameters were chosen as $\gamma_1 = \gamma_2 = \gamma$, $\gamma_3 = 0.01\gamma$, $\Delta_c = 0.9\gamma$, $C = 100\gamma$, and $\Omega_c = \gamma$.

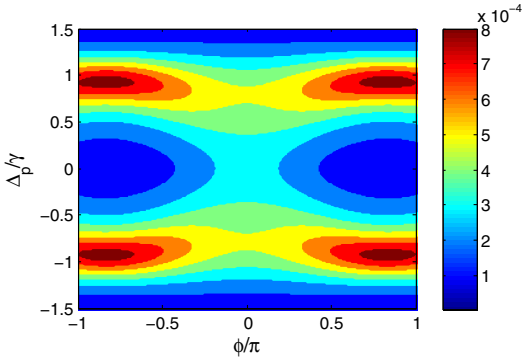

Fig. 7. Density plot of the probe absorption $\mathrm{Im}\,\rho_{23}$ versus the detuning Δ_p and the phase difference ϕ between two components of the polarized electric field of the EPF. Other values of the parameters were chosen as $\gamma_1 = \gamma_2 = \gamma$, $\gamma_3 = 0.01\gamma$, $\Delta_c = 0.9\gamma$, $\Omega_c = \gamma$, $\eta = 0.9$, and $\Omega_p = 0.01\gamma$.

parameters are kept fixed. Moreover, when the frequency detuning is changed from $\Delta_p = 0$ to $\Delta_p = \gamma$, and simultaneously the SGC effect is changed from $\eta = 0$ to $\eta = 0.9$, it was found from Fig. 6(d) that the phase difference ϕ plays an important role in the steady-state behavior. Compared with the curves ($\phi = 0$) in Figs. 6(a) and 6(b), Fig. 6(d) illustrates that the OB phenomenon can still be observed and the corresponding threshold increases slightly. When the relative phase is changed from 0 to $\pi/3$, the threshold of OB becomes more pronounced. In contrast to Fig. 6(c), it can be seen in Fig. 6(d) that the OM phenomenon appears when the relative phase ϕ is tuned to $2\pi/3$. In other words, in presence of the perfect SGC effect, we can easily realize a switch from OB to OM or vice versa just by adjusting the phase difference between the two components of the polarized electric field. These phenomena also demonstrate that the phase difference between the two components of the polarized electric field can effectively control the steady-state response in the present atomic system, which leads to the appearance of OM.

To obtain a better understanding of how the frequency detuning Δ_p and the phase difference ϕ between the two components of the polarized electric field of the EPF affect the steady-state behavior, we drew a density plot of the probe absorption $\mathrm{Im}(\rho_{23})$ versus the frequency detuning Δ_p and the phase difference ϕ as shown in Fig. 7. The reason for these interesting phenomena that were shown in Fig. 6 can be found from the changes of the absorption properties illustrated in Fig. 7. In the absence of the SGC effect ($\eta = 0$), the probe field can transmit through the medium without absorption at the probing resonance position ($\Delta_p = 0$) when $\phi = 0$. In other words, the input field E_p^I is approximately proportional to the output field E_p^T, which results in the case without the appearance of the OB phenomenon. When the perfect SGC effect is included ($\eta = 0.9$), the large absorption of the medium at the probing resonance position results in the output of the OB phenomenon with $\phi = 0$. However, the probe absorption is shown to be negligible when the phase between the two components of the polarized electric field of the EPF ϕ is tuned to $2\pi/3$. Therefore, one can find from Fig. 6(a) that the OB phenomenon disappears again. However, if the frequency detuning Δ_p of the probe field is tuned to $\Delta_p = \gamma$, from Fig. 7, we can see that the absorption of the medium clearly increases, which leads to the appearance of the OB phenomenon as shown in Fig. 6(d). Especially, the corresponding absorption is dramatically enhanced under the condition of $\phi = 2\pi/3$, which causes the parameter y in Eq. (17) to not be a cubic polynomial of the variable x, and thus the OM phenomenon appears. Based on the absorption spectrum shown in Fig. 4, the results shown in Figs. 6(b) and 6(c) can also be understood clearly.

4. CONCLUSIONS

In conclusion, we have analyzed in detail the steady-state behaviors in a four-level Y-type atomic system driven coherently by a probe laser and a single EPF by means of a unidirectional ring cavity. It was clearly shown that a controllable OB can be achieved by adjusting different parameters in the present atomic system. Under the steady-state condition, the threshold intensity and related hysteresis cycle area for the OB can also be modified by modulating the frequency detuning of the probe field, the intensity of driving fields, and the atomic cooperation parameter, as well as the phase difference between the two components of the polarized electric field. To obtain the two components of the polarized electric field Ω_c^+ and Ω_c^- of the control field, one can let the control beam pass through 1/2 and 1/4 wave plates in turn properly [32]. After passing through the 1/2 wave plates, the vertical polarized beam can be obtained. The rotating angle ϕ can be modulated by the 1/4 wave plate. Thus, one can obtain the EPF containing the two components (i.e., Ω_c^+ and Ω_c^-). More interestingly, we demonstrate the switch from OB to OM with the existence of a perfect SGC effect. With these results, we believe that phase controlled OB and OM will provide another feasible approach for applications in quantum information science.

ACKNOWLEDGMENTS

The research was supported in part by the National Natural Science Foundation of China under Grant Nos. 11374050 and 61372102, by the Qing Lan project of Jiangsu, and by the Fundamental Research Funds for the Central Universities under Grant No. 2242012R30011.

REFERENCES

1. J. S. Peng and G. Li, *Introduction to Modern Quantum Optics* (World Scientific, 1998).
2. N. A. Ansari, J. Gea-Banacloche, and M. S. Zubairy, "Phase-sensitive amplification in a three-level atomic system," Phys. Rev. A **41**, 5179 (1990).
3. S. Y. Zhu, H. Chen, and H. Huang, "Quantum interference effects in spontaneous emission from an atom embedded in a photonic band gap structure," Phys. Rev. Lett. **79**, 205 (1997).
4. M. A. G. Martinez, P. R. Herezfeld, C. Samuels, L. M. Narducci, and C. H. Keitel, "Quantum interference effects in spontaneous atomic emission: dependence of the resonance fluorescence spectrum on the phase of the driving field," Phys. Rev. A **55**, 4483 (1997).
5. E. Paspalakis and P. L. Knight, "Phase control of spontaneous emission," Phys. Rev. Lett. **81**, 293–296 (1998).
6. S. Menon and G. S. Agarwal, "Effects of spontaneously generated coherence on the pump-probe response of a Λ system," Phys. Rev. A **57**, 4014 (1998).
7. P. Zhou and S. Swain, "Phase-dependent spectra in a driven two-level atom," Phys. Rev. Lett. **82**, 2500 (1999).
8. F. Ghafoor, S. Y. Zhu, and M. S. Zubairy, "Amplitude and phase control of spontaneous emission," Phys. Rev. A **62**, 013811 (2000).

9. J. Evers, D. Bullock, and C. H. Keitel, "Dark state suppression and narrow fluorescent feature in a laser-driven Λ atom," Opt. Commun. **209**, 173–179 (2002).
10. X.-M. Hu and J.-S. Peng, "Quantum interference from spontaneous decay in Lamba systems: realization in the dressed-state picture," J. Phys. B **33**, 921–931 (2000).
11. J. H. Wu and J. Y. Gao, "Phase control of light amplification without inversion in a Λ system with spontaneously generated coherence," Phys. Rev. A **65**, 063807 (2002).
12. Y. Bai, H. Guo, H. Sun, D. Han, C. Liu, and X. Chen, "Effects of spontaneously generated coherence on the conditions for exhibiting lasing without inversion in a V system," Phys. Rev. A **69**, 043814 (2004).
13. J. Javanainen, "Effect of state superpositions created by spontaneous emission on laser-driven transitions," Europhys. Lett. **17**, 407 (1992).
14. M. O. Scully and M. Fleischhauer, "High-sensitivity magnetometer based on index-enhanced media," Phys. Rev. Lett. **69**, 1360 (1992).
15. K. Hakuta, L. Marmet, and B. P. Stoicheff, "Electric-field-induced second-harmonic generation with reduced absorption in atomic hydrogen," Phys. Rev. Lett. **66**, 596 (1991).
16. S. E. Harris, "Normal modes for electromagnetically induced transparency," Phys. Rev. Lett. **72**, 52 (1994).
17. D. Cheng, C. Liu, and S. Gong, "Optical bistability and multistability via the effect of spontaneously generated coherence in a three-level ladder-type atomic system," Phys. Lett. A **332**, 244–249 (2004).
18. A. Joshi, W. Yang, and M. Xiao, "Effect of spontaneously generated coherence on optical bistability in three-level Λ-type atomic system," Phys. Lett. A **315**, 203–207 (2003).
19. C. Liu, S. Gong, X. Fan, and Z. Xu, "Phase control of spontaneously generated coherence induced bistability," Opt. Commun. **239**, 383–388 (2004).
20. S. Gong, S. Du, Z. Xu, and S. Pan, "Optical bistability via a phase fluctuation effect of the control field," Phys. Lett. A **222**, 237–240 (1996).
21. X. M. Hu and Z. Z. Xu, "Phase control of amplitude-fluctuation-induced bistability," J. Opt. B Quant. Semiclass. Opt. **3**, 35–38 (2001).
22. J.-H. Li, X.-Y. Lü, J.-M. Luo, and Q.-J. Huang, "Optical bistability and multistability via atomic coherence in an N-type atomic medium," Phys. Rev. A **74**, 035801 (2006).
23. A. Joshi, W. Yang, and M. Xiao, "Effect of spontaneously generated coherence on the dynamics of multi-level atomic systems," Phys. Lett. A **325**, 30–36 (2004).
24. A. Joshi, W. Yang, and M. Xiao, "Effect of quantum interference on optical bistability in the three-level V-type atomic system," Phys. Rev. A **68**, 015806 (2003).
25. X.-Y. Lü, J.-H. Li, J.-B. Liu, and J.-M. Luo, "Optical bistability via quantum interference in a four-level atomic medium," J. Phys. B **39**, 5161–5171 (2006).
26. M. Sahrai, S. H. Asadpour, H. Mahrami, and R. Sadighi-Bonabi, "Controlling the optical bistability via quantum interference in a four-level N-type atomic system," J. Lumin. **131**, 1682–1686 (2011).
27. Y. Wu and X. Yang, "Highly efficient four-wave mixing in double-Λ system in ultraslow propagation regime," Phys. Rev. A **70**, 053818 (2004).
28. Y. Wu, M. G. Payne, E. W. Hagley, and L. Deng, "Efficient multiwave mixing in the ultraslow propagation regime and the role of multiphoton quantum destructive interference," Opt. Lett. **29**, 2294–2296 (2004).
29. Y. Wu and L. Deng, "Achieving multifrequency mode entanglement with ultraslow multiwave mixing," Opt. Lett. **29**, 1144–1146 (2004).
30. M. Shapiro and P. Brumer, "Coherent control of molecular dynamics," Rep. Prog. Phys. **66**, 859 (2003).
31. J. F. Dynes and E. Paspalakis, "Phase control of electron population, absorption, and dispersion properties of a semiconductor quantum well," Phys. Rev. B **73**, 233305 (2006).
32. U. Khadka, Y. P. Zhang, and M. Xiao, "Control of multitransparency windows via dark-state phase manipulation," Phys. Rev. A **81**, 023830 (2010).
33. L. A. Lugiato, "II theory of optical bistability," Prog. Opt. **21**, 69–216 (1984).
34. D. Steck, http://steck.us/alkalidata.
35. Y. Wu, M. G. Payne, E. W. Hagley, and L. Deng, "Preparation of multiparty entangled states using pairwise perfectly efficient single-probe photon four-wave mixing," Phys. Rev. A **69**, 063803 (2004).
36. Y. Wu, "Simple algebraic method to solve a coupled-channel cavity QED model," Phys. Rev. A **54**, 4534–4543 (1996).
37. Y. Wu and X. Yang, "Effective two-level model for a three-level atom in the Ξ configuration," Phys. Rev. A **56**, 2443–2446 (1997).
38. W. X. Yang, J. M. Hou, and R. K. Lee, "Ultraslow bright and dark solitons in semiconductor quantum wells," Phys. Rev. A **77**, 033838 (2008).
39. W. X. Yang, J. M. Hou, Y. Y. Lin, and R. K. Lee, "Detuning management of optical solitons in coupled quantum wells," Phys. Rev. A **79**, 033825 (2009).
40. W. X. Yang, A. X. Chen, R. K. Lee, and Y. Wu, "Matched slow optical soliton pairs via biexciton coherence in quantum dots," Phys. Rev. A **84**, 013835 (2011).
41. A. Joshi and M. Xiao, "Optical multistability in three-level atoms inside an optical ring cavity," Phys. Rev. Lett. **91**, 143904 (2003).
42. A. Joshi, A. Brown, H. Wang, and M. Xiao, "Controlling optical bistability in a three-level atomic system," Phys. Rev. A **67**, 041801(R) (2003).
43. Z. P. Wang and H. Fan, "Phase-dependent optical bistability and multistability in a semiconductor quantum well system," J. Lumin. **130**, 2084–2088 (2010).
44. Z. Wang, A. X. Chen, Y. Bai, W. X. Yang, and R. K. Lee, "Coherent control of optical bistability in an open Λ-type three-level atomic system," J. Opt. Soc. Am. B **29**, 2891–2896 (2012).
45. S. H. Asadpour, M. Jaberi, and H. R. Soleimani, "Phase control of optical bistability and multistability via spin coherence in a quantum well waveguide," J. Opt. Soc. Am. B **30**, 1815–1820 (2013).
46. Z. P. Wang and B. Yu, "Optical bistability via dual electromagnetically induced transparency in a coupled quantum-well nanostructure," J. Appl. Phys. **113**, 113101 (2013).
47. J. M. Yuan, W. K. Feng, P. Y. Li, X. Zhang, Y. Q. Zhang, H. B. Zheng, and Y. P. Zhang, "Controllable vacuum Rabi splitting and optical bistability of multi-wave-mixing signal inside a ring cavity," Phys. Rev. A **86**, 063820 (2012).
48. H. B. Wu, J. Gea-Banacloche, and M. Xiao, "Observation of intracavity electromagnetically induced transparency and polariton resonances in a doppler-broadened medium," Phys. Rev. Lett. **100**, 173602 (2008).
49. Y. P. Zhang, Z. G. Wang, Z. Q. Nie, C. B. Li, H. X. Chen, K. Q. Lu, and M. Xiao, "Four-wave mixing dipole soliton in laser-induced atomic gratings," Phys. Rev. Lett. **106**, 093904 (2011).